HAL
archives-ouvertes.fr

The origin of duo-lateral position-sensitive detector distortions

M. Solal

▶ To cite this version:

M. Solal. The origin of duo-lateral position-sensitive detector distortions. Nuclear Instruments and Methods in Physics Research Section A: Accelerators, Spectrometers, Detectors and Associated Equipment, Elsevier, 2007, 572, pp.1047-1055. 10.1016/j.nima.2006.12.042 . in2p3-00145801

HAL Id: in2p3-00145801
http://hal.in2p3.fr/in2p3-00145801

Submitted on 14 May 2007

HAL is a multi-disciplinary open access archive for the deposit and dissemination of scientific research documents, whether they are published or not. The documents may come from teaching and research institutions in France or abroad, or from public or private research centers.

L'archive ouverte pluridisciplinaire **HAL**, est destinée au dépôt et à la diffusion de documents scientifiques de niveau recherche, publiés ou non, émanant des établissements d'enseignement et de recherche français ou étrangers, des laboratoires publics ou privés.

The origin of duo-lateral position sensitive detector distortions

M. Solal.

Institut de Physique Nucléaire d'Orsay - CNRS, Université Paris-Sud, Bat.106, 91406 ORSAY Cedex, France

Abstract

Duo-lateral Position Sensitive Detectors (PSD) are used for their low intrinsic distortion. This PSD was used for the γ camera POCI (Per Operative Compact Imager) dedicated to the detection of body tumour. Besides, we developed a simulation model of this PSD. Our objective is to optimise PSD and readout electronics parameters in order to improve residual spatial non linearity, especially in detector edges. Various simulations runs based on our model were performed. The corresponding results are very close to experimental observation. Finally, this simulation is a powerfull tool for analysing PSD behaviour in particular cushion distortions.

PACS :

Keywords : PSD ; Continuous position sensitive detector ; model ; simulation ; distortion

I. Introduction

In some applications, when multiplicity (number of incident particles) and counting rate are not critical, it is well suited to use a silicon continuous Position Sensitive Detector (PSD) for locating particles, the active area is up to 60 mm x 60 mm. Continuous PSD are available in standard devices and only four to five electronics channels are needed for the readout of the whole surface of detection and high spatial resolution is achieved when incident particles are at high energy [1, 2]. PSD can be associated with an image intensifier tube (IPSD) and a crystal plate for gamma rays detection [1, 3] or can be used directly to localize particle beam or heavy nuclei (alpha, carbon, phosphor, etc …). For example, an alpha particle of 5.5 MeV gives a typical spatial resolution of 1 mm (FWHM) for a PSD alone and 300 μm (FWHM) for an IPSD.

Since the first PSD development which began in the sixties, spatial non linearity has been largely observed [1..4]. In previous works, algorithms were used to correct spatial aberration [4] but the origin of the distortion has not yet understood; this is particularly true for the duo-lateral detector where the observed cushion distortion is not in accordance with this PSD geometry. In this paper, we will briefly recall the principle of continuous PSD and describe the simulation model we developed. The distortions observed experimentally will be compared to simulation results. Then the origin of the distortion will be analysed and explained. This study will allow choosing optimum PSD parameters for POCI (Per Operative Compact Imager) [1 .. 3, 5].

II. Method.

II.A. Principle

The continuous PSD is a 500 µm thick fully depleted diode of a large area, the distances between the electrodes define the active surface L x L (Fig. 1). For pin-cushion PSD, the front surface is covered by P+ ion implanted resistive layer: the corresponding resistance expressed in Ohm / square is R_{sq}= 10 to 22 kΩ. In integrated devices, a film resistor of thickness *d*, length *L* and the width *W* has a resistance $R = \rho \frac{L}{d \cdot W} = R_{sq} \frac{L}{W}$, where the ratio *(L/W)* is sometimes called the number of squares. Notice that the resistance *R* is independent of the sizes of the square. The back side is formed by a metallic cathode (Fig. 1): such PSD type shows strong distortions. In corrected pin-cushion PSD the four electrodes are linked via a low resistive deposited strip (Fig.1) with resistance typically ~ 2 kΩ [4]. The low resistive strip reduces the classical spatial distortion but causes a strong thermal noise [5]. In duo lateral PSD both sides are ion-implanted resistive sheets R_{sq} = 4 to 10 kΩ/sq; there is a bore implantation for the P+ side and a phosphorus implantation for the N side. The X location is measured on the bore side while the y location is measured on the phosphorus side (Fig. 1.b).

All PSD (Tetra lateral, pin cushion or duo lateral) are based of the same location principle; each electrode receives a fraction i_i of the total induced current due to drift of e-h pairs generated by incident particle. Induced current are integrated in a charge preamplifier.

For duo-lateral detectors, the determination of X and Y incident particle positions is based on the following relationships: $Q_{e1} = Q_t.(L/2+X)/L$,

$Q_{e2} = Q_t.(L/2-X)/L$,

$Q_{h1} = Q_t.(L/2+Y)/L$,

$Q_{h2} = Q_t.(L/2-Y)/L,$

where the origin is at the centre of PSD, $Q_t = Q_{e1} + Q_{e2} = Q_{h1} + Q_{h2}$ is the total charge collected, L is the PSD dimension.

For pin-cushion detectors, Q_{e1} is replaced by $Q_{ec} + Q_{ed}$,
Q_{e2} by $Q_{ea} + Q_{eb}$,
Q_{h1} by $Q_{ea} + Q_{ec}$
and Q_{h2} by $Q_{eb} + Q_{ed}$.

The position measurement is then given by:

$$\begin{pmatrix} X \\ Y \end{pmatrix} = \frac{L}{2} \cdot \frac{1}{Q_t} \cdot \begin{pmatrix} Q_{e1} - Q_{e2} \\ Q_{h1} - Q_{h2} \end{pmatrix}, \qquad (1)$$

$Q_t = Q_{ea}+Q_{eb}+Q_{ec}+Q_{ed} = Q_{e1}+Q_{e2} = Q_{h1}+Q_{h2}$ is proportional to the total energy deposited on the PSD. For pin-cushion PSD it is better (smaller noise and ballistic deficit) to measure Q_t from the backside.

II. B. Spatial resolution

Spatial FWHM resolution in both planes is given by

$$\delta(U) = 2.355 \cdot \left(L^2 \frac{1 + (\frac{U}{L/2})^2}{Q_E^{\,2}} . dQ_i^{\,2} \right)^{1/2}, \qquad (1.2)$$

where U = X or Y and dQ_i is the Equivalent Noise Charge (ENC) on a position electrode [5].

The main contribution to ENC is the Johnson noise ($2kT/R_{det}$) due to the low value of the resistive layer. Other noise contributions can be quadraticly added, for a CR-RC2 filter the equivalent noise charge is

$$ENC = \frac{1}{0.271} \left[\frac{2kT}{R_{det}} \tau + e_s \left(\tfrac{1}{16} \cdot \frac{C_{det}^{\,2}}{\tau} + \tfrac{3}{16} \cdot \frac{1}{R_{det}^{\,2}} \tau \right) + \tfrac{3}{16} \cdot qI_{leak} \tau + \tfrac{1}{4\pi} \cdot 2\pi A_f C_{det}^{\,2} \right]^{\frac{1}{2}}.$$

The prefactor normalizes the noise to the signal gain, the second term combines the serial noise of the preamplifier e_s and the detector impedance (capacitive and resistive part), and the last term is the contribution of excess noise [5, 6].

Formula of spatial resolution (1.2) is perfectly verified by experiments [2]. If the charge is not completely collected (ballistic deficit mode) due to a too short integration time constant, the formula (1.2) should be replaced by

$$\begin{pmatrix}\delta(X)\\ \delta(Y)\end{pmatrix}=2.355\cdot\frac{L\cdot ENC}{\left(\sum_{i=A}^{D}Q_i\right)^2}\cdot\sqrt{2}\cdot\begin{pmatrix}\sqrt{(Q_C+Q_D)^2+(Q_A+Q_B)^2}\\ \sqrt{(Q_B+Q_D)^2+(Q_A+Q_C)^2}\end{pmatrix},$$

where Q_i is the effective charge collected [5].

II.C. Spatial distortion

Spatial non linearity is often observed on two dimensional detectors. This effect is inherent to the geometry of the PSD and the electronics readout. Moreover, the observed distortion increases when the time constant of the spectroscopy filter decreases. A higher time constant reduces the distortion but increases the parallel noise contribution and hence degrades the spatial resolution [5].

The electrodes configuration is shown in Fig. 1 for a duo-lateral and a pin-cushion detector. To evaluate the spatial linearity of the PSD, a thick lead mask perforated by an array with 5 mm spaced 1 mm holes was put on the front surface of the PSD. A ^{241}Am source, placed at 20 cm distance from the mask, irradiated the whole detector (fig. 2.a). In the case of pin-cushion detectors, the strong distortion is simply linked to the geometrical configuration of the electrodes (fig. 2.b) [7]. In the case of duo-lateral detectors the weak distortion could not be attributed to the position of the electrodes which are parallel to each other.

In our knowledge, there is no analytical solution allowing to analyse the observed distortion in duo-lateral PSD. The resistive sheet and capacitance are continuously distributed, then, based on the finite element model of R.L. Cowin [6] (numerical computation), M. Solal [5] developed an electronics model simulated with Spice software.

II.D. Charge sensitive preamplifier

The deposited energy induces current which flow to the four input channels via the resistive sheet. The resistive sheet seen by the preamplifier also requires suitable electronics. As illustration, we present in Fig. 3.a. the deficit signal versus the resistive input for a standard charge sensitive amplifier (CSA) and the electronics principle (Fig. 3.b) implemented in POCI camera to suppress the deficit signals. The complete diagram of the designed CSA is given in Fig. 4. It should be stressed that in order to quantify the intrinsic distortion of the PSD, we used a perfect charge sensitive preamplifier in our simulation model (e.g., input impedance Z_{in} = 0 Ω, the time integration constant τ = 0 and the sensitivity = $1/C_f$). Further the contribution of the input impedance will be taken in a second model.

III. Simulation model

III.A. PSD

In a previous paper [5] the model included 13 x 13 cells. Numerical simulations were performed for the two kinds of pin-cushions PSD. For the 300 µm thick duo-lateral PSD of 42 x 42 mm^2 area, the previous model was completed with two resistive layers R_{bore} and $R_{phosphore}$, which are linked by the distributed diode capacitance (Fig. 5.a). A particular attention was paid to the edges (Fig. 5.b), and especially in the area around the contact electrodes where the main unexpected distortions are located. More precisely, metal contacts overlap P and N^+ layers (Fig 5.b). In order to reproduce with sufficient accuracy these weak spatial non lineraties, the number of cells was increased to 15 x 15. The active area L x L is divided into 15 slices of equal width $\Delta X = \Delta Y$, to simulate the spatial response a current pulse was injected at the different cell nodes. The whole model is implemented in OrCad Capture CIS 10.3 software and simulated with using OrCad PSpice 10.3 software (distributed by Advanced Logic System Design, http://www.alsdesign.fr).

III.B. Filters

The first simulation was performed without spectroscopy filter, directly at the charge preamplifier output in order to show PSD intrinsic distortions. In the subsequent simulation we will introduce the filter in order to analyse the observed experimental spatial distortion. The spectroscopy filter used in experiment is the Ortec 571 (Fig. 6) which is implemented with PSpice “Analog Behaviour Model” block. The exact transfer function *T(s)* is

$$T(s) = 2{,}84013 \times \frac{\tau \cdot s}{1+\tau \cdot s} \times \frac{1}{1+\frac{\tau}{3}\cdot s} \times \frac{1}{1+\frac{2\cdot\tau}{1+k^2}\cdot s + \frac{\tau^2}{1+k^2}\cdot s^2} \quad ,$$

where k = 0,8 and τ = 600 ns [8].

IV Results

IV.A Simulated intrinsic PSD response

In this section we will focus on the analysis of the simulated intrinsic non linearities of the duo-lateral PSD. The modelled PSD (300 µm thick) is considered fully depleted, in experiment the full depletion voltage is 30 Volts. The determination of the centroïd is performed directly at the charge sensitive preamplifier (CSA) output. As described in previous section (§ II.D), this component is assumed perfect. Consequently the charge collected at the preamplifier is directly proportional to the integral of the current flowing through the contacts which are short circuited. The simulated CSA output waveforms (taken from the bore electrode) are represented in Fig. 7 for different positions 3 mm spaced along X axis. We can notice a very long establishing time (~ 1µsec) even for a particle hitting just near the electrode x1 (X=L/2), however the asymptotic values are strictly linear of X.

The simulated mapping response is obtained by injecting the current source in each nodal mesh (15 x 15 nodes) of equal 3 mm spacing $\Delta X = \Delta Y$. The normalized coordinates are noted $x = X / (L/2)$ and $y = Y / (L/2)$. The centroïd (x, y) is calculated for each source position and the corresponding dot is plotted in Fig. 8. The calculated position patterns of the PSD modelled (Fig. 8) calls for two comments:

1) Contrary to experimental observations, an unexpected barrel distortion is clearly observed!
2) The maximum calculated centroïd at edges is 1.5 in y and 1.2 in x, instead of the theoretically maximum values $x=\frac{V_{x1}-0}{V_{x1}+0}=1$ and $y=\frac{Vy_1-0}{Vy_1+0}=1$

A first conclusion would be addressed: the intrinsic calculated PSD distortions (based on this first model) are far from the experimental observation.

Using this first model, centroïds are calculated with potentials taken at t = 500ns (V_{x1} *(t=500ns)* and V_{x2} *(t=500ns))* corresponding to the collection time of the shaping amplifier. The unexpected distortion results from the data processing procedure. Some values of V_{x2} *(t=500ns)* observed are small and negative for a hit near the electrode x_1, then, the centroïd $x = \frac{V_{x1}-V_{x2}}{V_{x1}+V_{x2}}$ could be greater than 1 (with $V_{x2}<0$ *instead of 0)*. Bipolar current pulses on the x2 electrode are expected. The current of opposite sign in two dimensional duo-lateral PSD was measured by E. Lægsgaard for $t/(R_{det}C_{det}) < 0.2$ at certain positions [8]. This phenomena was studied by A. J. Tuzzolino who called it “anomalous” current and calculated it in a particular case [10]. The induced current calculation in silicon has been studied for non-grounded electrodes by E. Gatti et al. [11].

Figure 9 shows two responses for different values of y and the same x=1, one of the curves is obtained by simulation for a particle hitting the middle of the electrode and the other one for a particle hitting the electrode edge. In these cases, we expect a short collection time corresponding to 10 ns drift time, this is not the case and we notice two different collection times. We will see in the next paragraph that these different settling times have an effect in the spectroscopy amplifier and explain the distortion. Figure 10 shows the difference in charge collection between bore and phosphorus sides.

The bipolar current pulse and the long collection times are specific to duo-lateral PSD and don't exist in one dimensional PSD neither in pin-cushion or tetra-lateral PSD. The reason for this phenomenon is the both sides are resistive and are capacitively coupled. Such behaviour in pin-cushion PSD is much smaller due to metal plane. Both resistive sheets of duo-lateral PSD are not grounded, that it is explained in figure 11. The drift current is modelled by a current source, with one of its terminal connected close to the preamplifier and the other terminal connected to the resistive sheet. Then, the current flowing into the preamplifier for a particle near the bore electrode is given by

$$i_{bore} = i_{source} \times \frac{1}{1 + j.C_c.\omega.\left(Z_{phos1} // Z_{phos2}\right)}, \qquad (1.a)$$

and for phosphorus side it is given by

$$i_{phos} = i_{source} \times \frac{1}{1 + j.C_c.\omega.\left(Z_{bore1} // Z_{bore2}\right)}. \qquad (1.b)$$

Cc is the local coupling capacitor, *Zphos1* is the impedance between one of the terminals of i_{source} and the electrode 1 of the phosphorus side. *Zphos2* is the impedance between the same terminal of i_{source} and the electrode 2 of the phosphorus side.

Then, the current flowing to the preamplifier can't be instantaneous, the time constant is C_cZ with $Z = Z_1 // Z_2$ which depends on the position, thus explaining the waveforms found in figures 7 to 10 which correspond to the integrated currents. The simulated current for a hit of the phosphorus electrode is given in figure 12, the current collected by the preamplifier connected to the phosphorus electrode is effectively not equal to the drift current. On the opposite electrode, the bipolar current pulse with integral 0 is found, after 500 ns the current turns to positive.

IV. B. Response with shaping amplifier

The filter amplifier described in paragraph III.B, is now connected at the output CSA preamplifier. Figure 13 shows the output voltage response of the filter along x and y axes. We see that the bipolar pulse of the CSA output voltage has an effect onto the response of the spectroscopy amplifier. For positions near the opposite of the collection electrode, the output filter has a bipolar pulse shape. For x or y = -1, the pulses do not stay at the expected value zero. In this case, the maximum sampled value (positive in boron side) leads to calculate a centroïd value smaller than the expected hit position. We see the same effect for the phosphorus side with opposite signal polarity. We can also notice a more important effect on the phosphorus side than on the boron side.

The spatial linearity of the shaping amplifier is given in fig. 14 for incident positions on equidistant lines along the x and y directions. The simulated response is now in good agreement with experimental mapping in all regions. The ovoid points are due to the difference in resistive layers, the phosphorus side is noisier [5]. Spatial distortions are more important along y axis corresponding to the phosphorus channel. This could have been predicted by observing figure 11, the centroïd value for a hit at x=1 is given by

$x = \frac{v_{max}(x=1) - v_{max}(x=-1)}{v_{max}(x=1) + v_{max}(x=-1)} = \frac{29.3 - 0.9}{29.3 + 0.9}$, this value is lower than the expected centroïd value x=1. For a hit at y=1, the determination of the centroïd value is

$y = \frac{-v_{min}(y=1) + v_{min}(y=-1)}{-v_{min}(y=1) - v_{min}(y=-1)} = \frac{27.7 - 1.8}{27.7 + 1.8}$, which is lower than y =1.

The difference in shape for phosphorus and bore channel is a consequence of the difference in charge collection time. The charge collection time is given in first approximation by equations (1), this collection time on the bore side is determined by the resistance of the phosphorus sheet (4 kΩ) and the collection time on the phosphorus side is determined by the resistance of the boron sheet (8 kΩ). The collection time is function of the resistive layer of the opposite side. A short collection time reduces the ballistic deficit, then the distortions on the boron side are less important because the resistance of the phosphorus sheet is lower and vice versa (Fig. 14). The position pattern obtained by experiment in figure 15 confirms this explanation, spatial linearity is improved in both side by $R_{ph} = R_{bo} = 4$ kΩ and only in y direction by $R_{ph} = 8$ kΩ and $R_{bo} = 4$ kΩ. Therefore a distortion on one side could be reduced by reducing the resistance sheet of the other side. In our application POCI (Per Operative Compact Imager) a duo-lateral PSD with resistive layers $R_{ph} = R_{bo} = 4$ kΩ have been implemented.

IV.C. Improvement

The input impedance of the preamplifier has also been tested. This has been performed by introducing a resistance in parallel with the perfect preamplifier. The results show a degradation of the existing distortion as the input impedance increases. In order to improve the linearity the input impedance of the preamplifier should be as small as possible.

The spatial linearity could be improved by increasing the collection time as discussed in section V.a, or/and by reducing the value of the resistive sheet $R_{detector}$. This is realized by increasing the depth of ion implant. But these two solutions lead to an increase of the parallel noise (thermal noise) leading to a bad spatial resolution [5].

An alternative solution consists of keeping a value not too small for the resistive sheet, between 8 kΩ to 30 kΩ to avoid a higher thermal current noise $2kT/R_{detector}$, and improving the front end electronics. The duo-lateral PSD needs electronics with a long collection time to avoid ballistic deficit and a short derivative time to reduce parallel noise. The solution adopted for POCI γ camera which is clinically evaluated [2] is the linear pseudo trapezoidal filter [12]. This solution was also used for gamma ray detection in large germanium detector [13] where the problematic is similar. The drift time is related to the distance of carriers travel leading to the ballistic deficits. For the trapezoidal weighting function the width of the constant portion determines the charge collection time, and the width of the two triangular portions is determined by the noise corner time constant [13]. Two-dimensional PSD readout by a trapezoidal filter has been studied by M. Solal, a constant portion width of about four times larger than the triangular width offers the best trade off between spatial resolution and position linearity [5]. But the large width of the constant portion leads to make a linear electronic design with an important number of Salen-key structures [12] and with some difficulties for the practical realisation du to the accuracy of components.

A time variant filter approach is the gated baseline restorer which has been studied and developed by Z. Zojceski [14], the output CSA is integrated during the time where the gate is open, the time derivation is given by the short time of the end of the gate. The gate duration must be adapted to reach the compromise between the ballistic deficit reduction and the noise integration, a pre-filter may be required. L. Fabris has developed a new pulse processing technique combining ballistic deficit immunity and resilience

to parallel noise [15], this time variant filter has been tested on a CdZnTe detector where the charge pulses collected have different shapes due to the impurities in the semi conductor.

A new idea based on progress in numerical sampling, is to keep a classical analogue invariant time filter (semi Gaussian or pseudo trapezoidal) and to sample the whole pulse shape. Thereby, any value of the pulse can be held at any time instead of holding the maximum value with a peak detector, classically used to have the maximum signal to noise ratio. We see obviously in figure 13 that the pulse shapes are not linear functions of x or y positions. This consideration could be used for reducing the distortion [16]. Let us consider a hit located at x = 1, the corresponding pulse value response at time t = 2.0 µsec gives for the centroïd the exact position x = $\frac{v_{t=2\mu s}(x=1)-v_{t=2\mu s}(x=-1)}{v_{t=2\mu s}(x=1)+v_{t=2\mu s}(x=-1)}=\frac{23.7mV-0}{23.7mV+0}$ = 1. We can notice at t = 2.0 µsec that the pulses pattern $v_{t=2.0\mu s}(x_i)$ improve considerably the linearity along whole the x axis. We also notice figure 13 that the same time t = 2.0 µsec gives also the optimum linearity along the y axis. In this solution the noise is unchanged because the signal is yet filtered by the spectroscopy amplifier but the signal is smaller at certain positions and then the signal to noise ratio is degraded by a factor less than 1.3. This solution is also very versatile, the signal to noise ratio is slightly degraded but the sampling allows choosing the optimum time which had the minimum spatial distortion.

V. Conclusion

The model developed allows prediction of the position non linearity. The results are in good agreement with experimental responses, reproducing all weak distortion in all regions. The model was used to optimize the sheet resistances of the PSD used for the POCI camera. Other parameters could be added. I.e., in gamma ray detection the IPSD [2] could be simulated by introducing the spatial repartition of the light spot and its time constant coming from the crystal plate. The preamplifier and its input impedance can be simulated at the component level.

The simulation model developed has allowed to a large extent to understand the exact origin of the distortion of the duo-lateral PSD. The long collection time and the bipolar current pulse are due to the resistive sheets at both sides in the duo-lateral PSD. Therefore the pulse shapes at the output of the spectroscopy amplifier depend on the hit location, leading to the spatial distortion. We can conclude that the classical readout by taking the maximum value of the shaping amplifier is the origin of the distortion largely observed, that readout is not well adapted for the duo-lateral PSD. The model presented is now validated and becomes a powerful tool to study alternative pulse processing in order to avoid distortions.

PSpice simulations performed in time domain allow also studying any time variant filter processing. One idea is to numerically exploit the whole sampled shape of the pulse which is effectively dependent on the position.

Acknowledgments: The author acknowledges Nguyen Duy of Sté Protec-Feu Nancy for the numerous Pspice simulations and S hanie Pitre of I.M.N.C. Orsay Paris XI for the exhaustive experimental measurements.

References

[1] L. Ménard, thèse Université Versailles (19 janvier 1999)

[2] S. Pitre, thèse Université Versailles (19 décembre 2002)

[3] L. Menard & al. IEEE Tr. Ncl. Sc. Vol. 44, No 3 (1998), p. 1293.

[4] M. Bruno & al. NIM A 311 (1992) 189

[5] M. Solal & al. NIM A 477 (2002) 491

[6] R.L. Cowin & al. NIM A 399 (1997) 365

[7] E. Lisi & N. Colonna NIM A 348 (1994) 703

[8] Model 571 Spectroscopy Amplifier Manual, EG&G Ortec Part No 733490, U.S.A.

[9] E Lægsgaard, Nucl. Inst. And Meth. 162 (1979) 93

[10] A.J. Tuzzolino, Nucl. Inst. And Meth Volume 70 (July 1988)

[11] E. Gatti, G. Padovini and V. Radeka, Nucl. Instr. and Meth. 193 (1982) 651.

[12] F.S. Goulding & D.A. Landis, IEEE Trans. Nucl. Sci. Vol 41, no. 4, August 1994.

[13] V. Radeka, NIM A 99 (1972) 525

[14] Z. Zojceski & al, NIMA 485 (2002) 645

[15] F. Lorenzo, 2000 IEEE Nucl. Sci. Symp. and Med. Imag. Conference, Lyon (FR)

[16] R. Selem, LCAM 91406 Orsay, private communication.

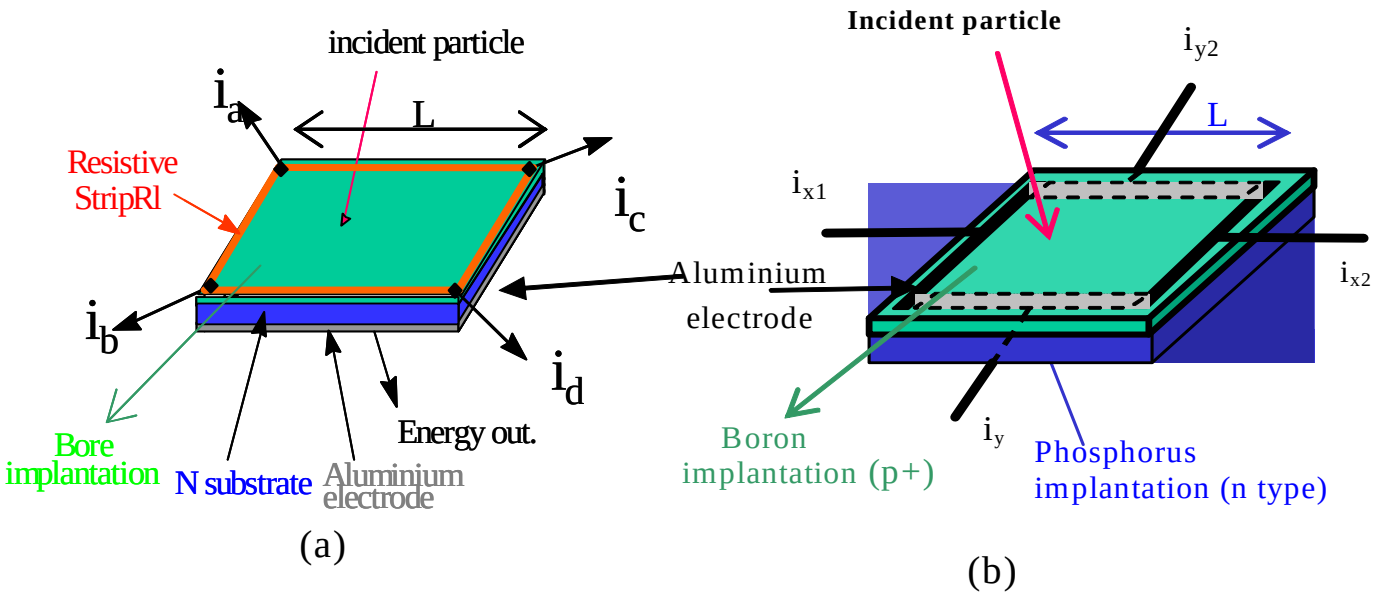

Fig. 1. PSD types: (a) in pin-cushion PSD the front side is a resistive sheet; the signals are taken at the four metallised contacts located on the corners and are used to determine the position. The back side is a metallic contact film used to improve the energy resolution. Without resistive strip Rl (standard detector), the spatial resolution is high but the spatial linearity is very bad. With a resistive strip the response is quite linear while the spatial resolution is degraded. (b) In duo-lateral PSD both sides are resistive with contacts located at the four edges on both sides (and orthogonally); this kind of PSD offers both a quite good spatial resolution and a good spatial linearity; but the drawback of this detector is the poor energy resolution (no metallic sheet).

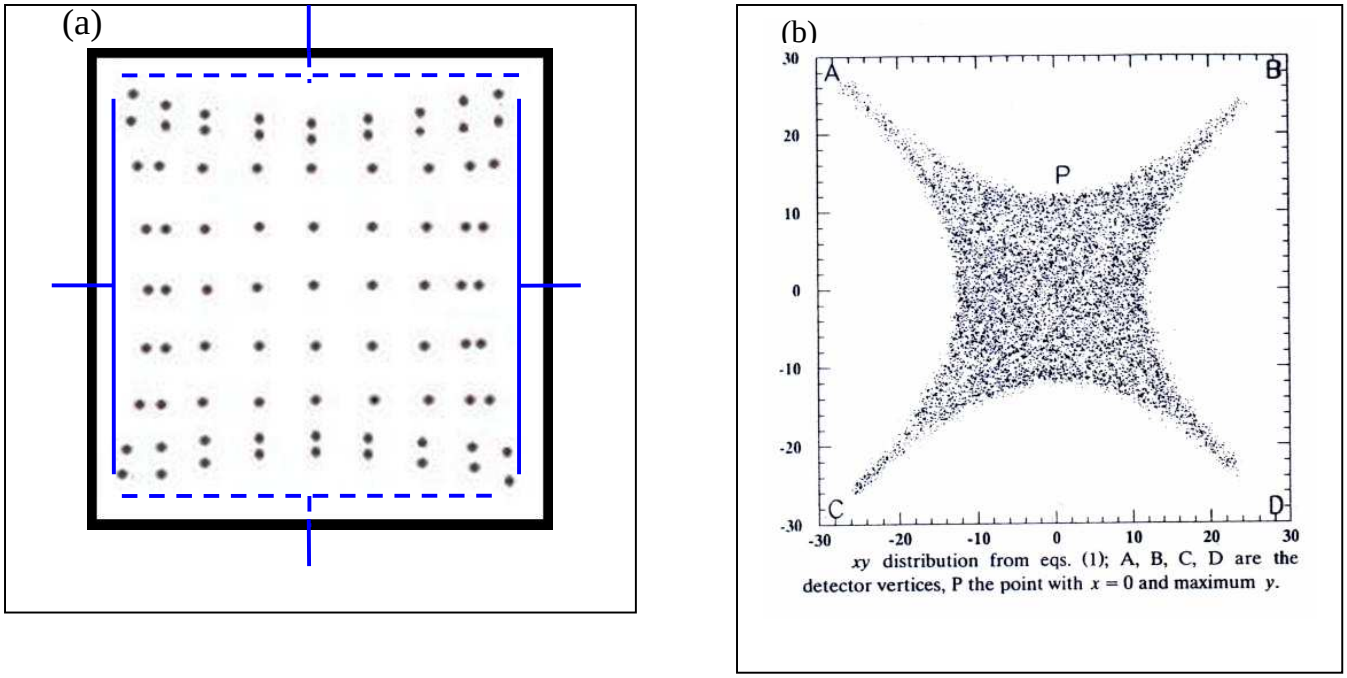

Fig. 2. Typical spatial distortion for a duo-lateral PSD (a) and for a pin-cushion detector (b) [7]. Note that a stronger distortion is observed in the case of pin-cushion detector: this is mainly due to the geometrical configuration of the electrodes [7]. A weak pin cushion distortion (Fig. 2.a) is observed near the edges for duo-lateral PSD, which can't be explained by electrode positions.

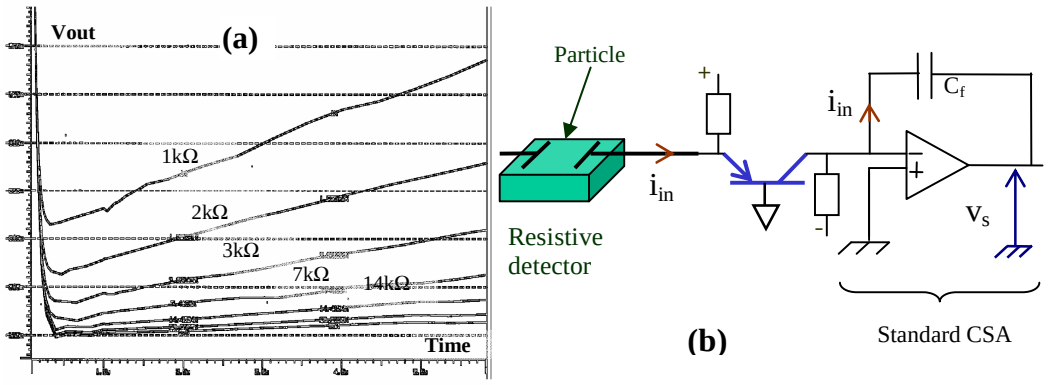

Fig. 3. (a) The signal lost with a standard charge sensitive preamplifier for different impedance resistive detector. (b) The principle used for POCI gamma camera; a common based transistor converts low resistive sheet impedance into high impedance; this solution avoids deficit signal but introduces noise due to the emitter resistor.

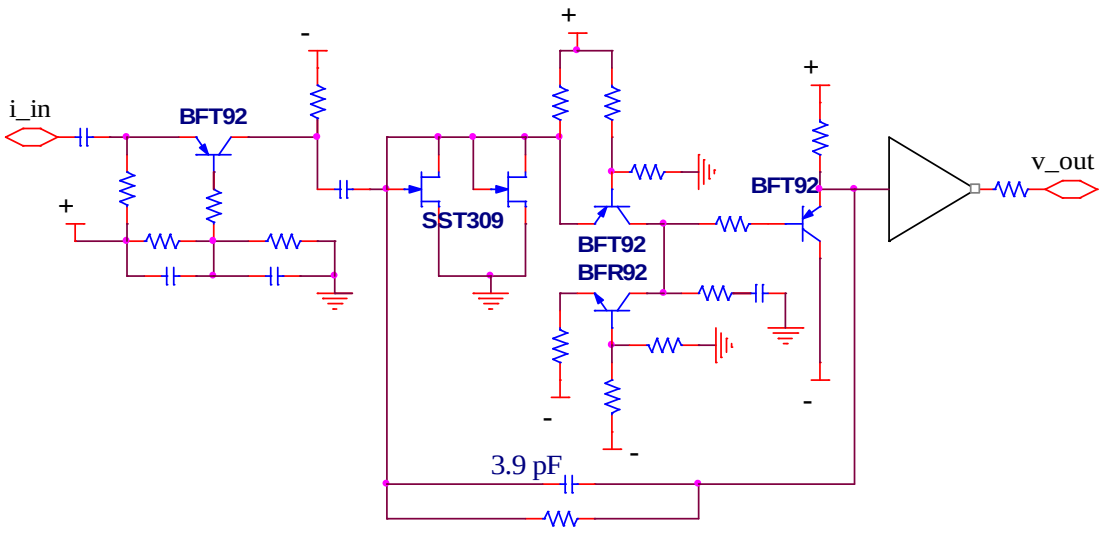

Fig. 4: Main elements of an electronic channel of the front side detector. The electronic channel of the rear side is the same expect for the type of the input and output transistor (feed-back) due to the opposite input polarity signals.

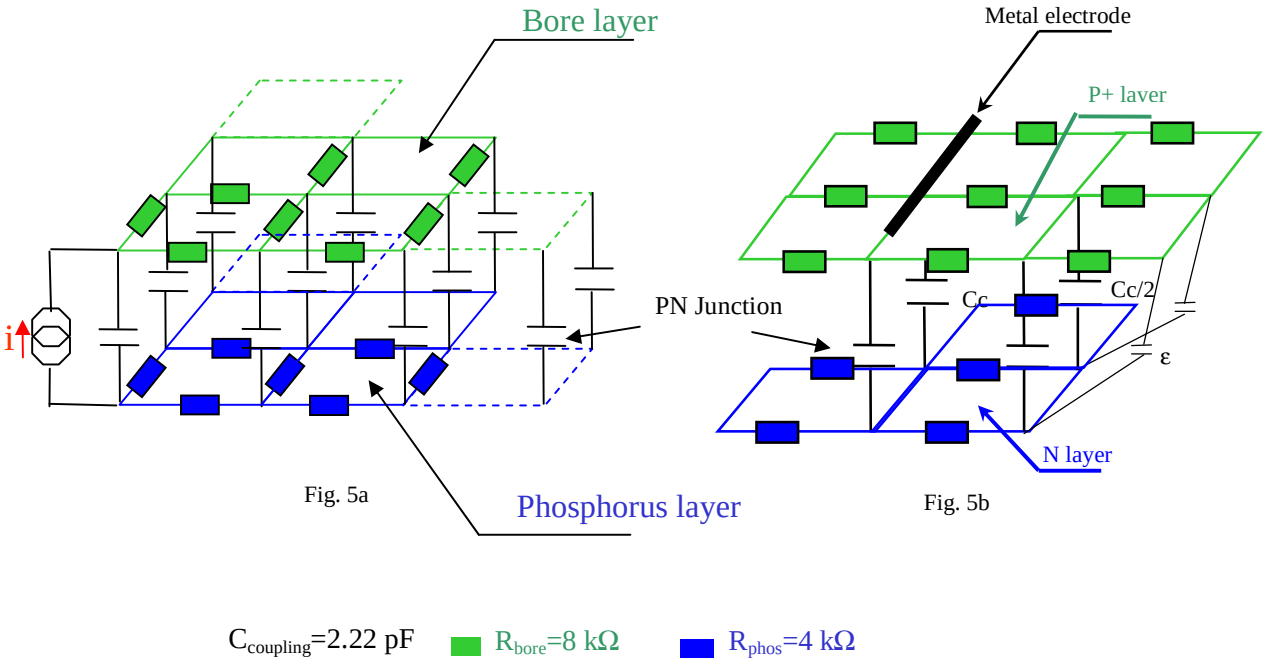

Fig. 5a. Duo-lateral continuous PSD model includes 15 x 15 cells which cover an active area of 45 x 45 mm^2, two resistive dividers are used, for the front side and for the back side. Fig. 5b. Near contact electrodes, distortions are more important and unexplained; a particular attention is paid in this region: metal contacts overlap P+ and N layers, junction capacitance is surrounding active region.

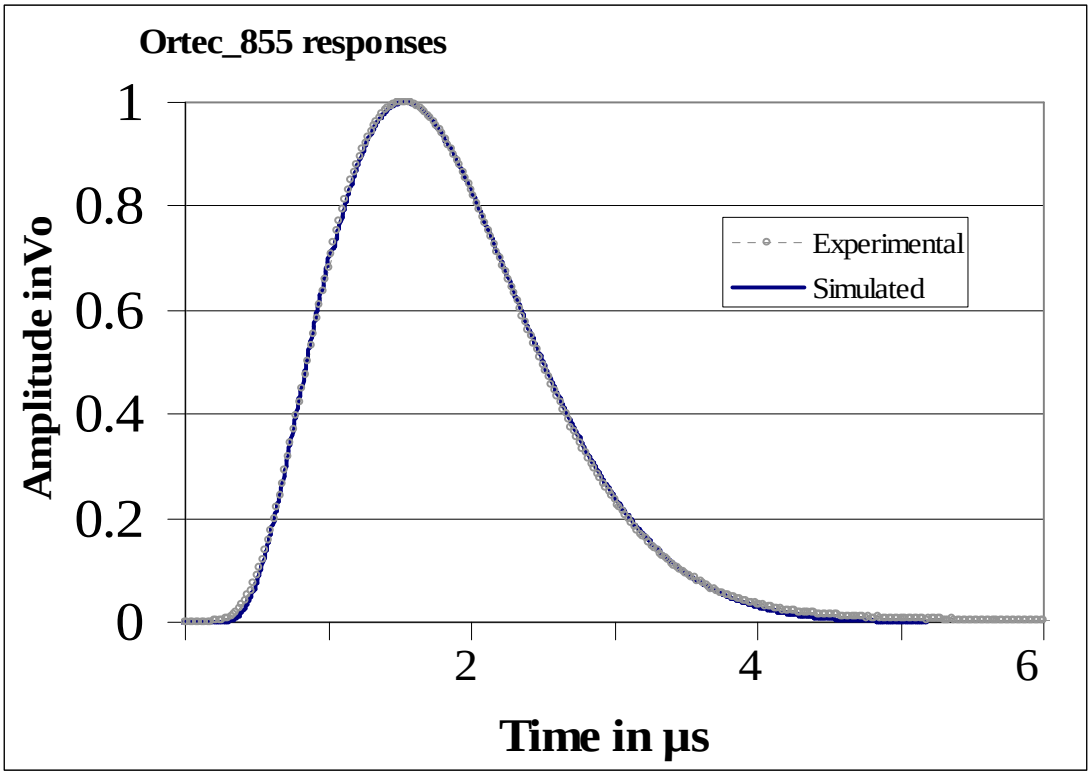

Fig. 6: The real and simulated time step response of the shaping amplifier; time constant τ = 600 ns and k=0.8. The transfer function is implemented by using elementary Laplace blocks from «Analog Behaviour Model» of Pspice library.

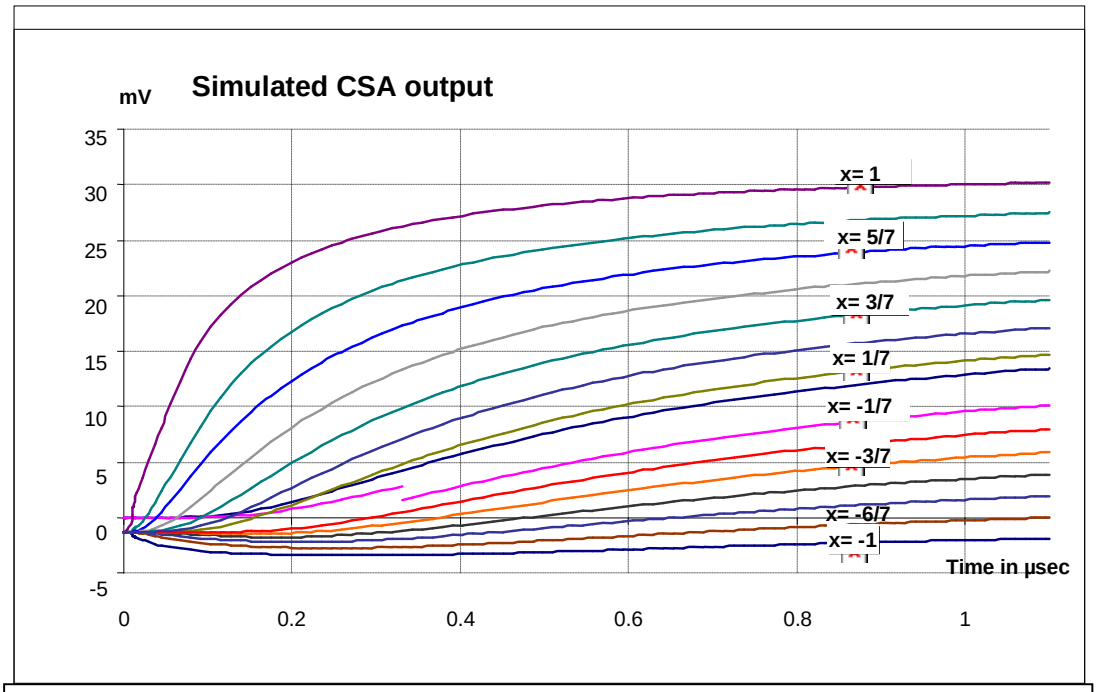

Fig. 7. Charge sensitive preamplifier waveforms $V_{x1}(X)$ along X axis. In this figure the normalized coordinate is noted x = X / (L/2). Far away from the electrode (x ~ -1) the negative signal corresponds to the integration of a negative current. After 1 µs the output voltages aim to the good values. As we can see, $V_{x1}(x=-6/7)$ turns positive and $V_{x1}(x=-1)$ goes to the normal value 0. Lastly, we notice a long and anomalous collection time even for a hit on the electrode (x=1)!

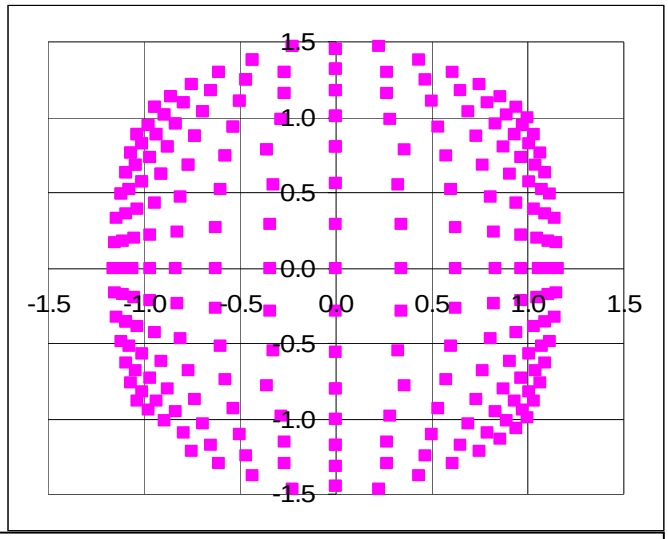

Fig. 8. Position pattern reconstruction of the PSD modelled. Each dot is the calculated position of nodal hit using the simulated amplitudes signals (V_x, Vy) at outputs of perfect charge sensitive preamplifiers. Due to the very long collection time, the charge is taken at t = 500 ns which corresponds to the collection time amplifier. We notice a barrel distortion which is the opposite of the expected “pin-cushion” distortion. Lastly, at edges, maximum calculated coordinates are greater than 1, which is theoretically not possible!

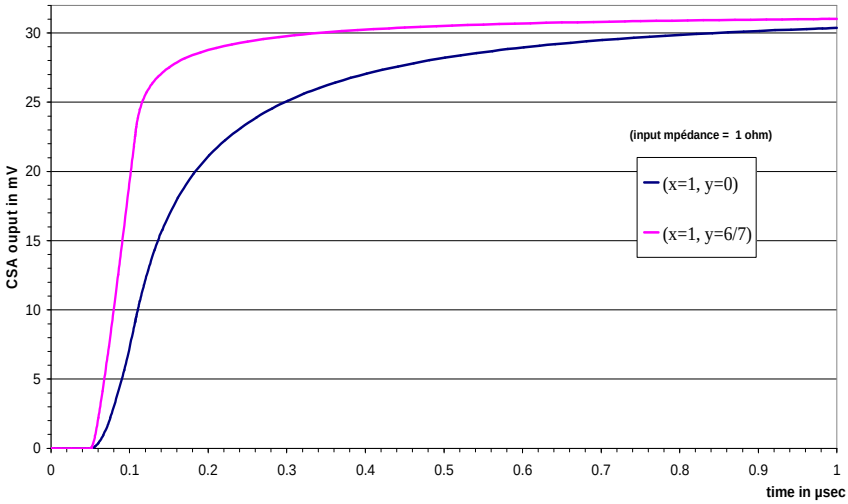

Fig. 9. CSA voltage output near (onto) the electrode corresponds to a location x=1 for y =0 and for y = 6/7 (in the middle and at the end of borus side electrode). The collection times are different, *V(x=1)* depends on y value; the settling time is longer in the middle of the PSD where the distortion is maximum. Because the voltage is taken before the complete settling at t=450ns the distortion shows up. Nevertheless, when a particle hits near the electrode (onto the electrode in this simulation) we expect an instantaneous collection time as it is observed on one dimensional PSD.

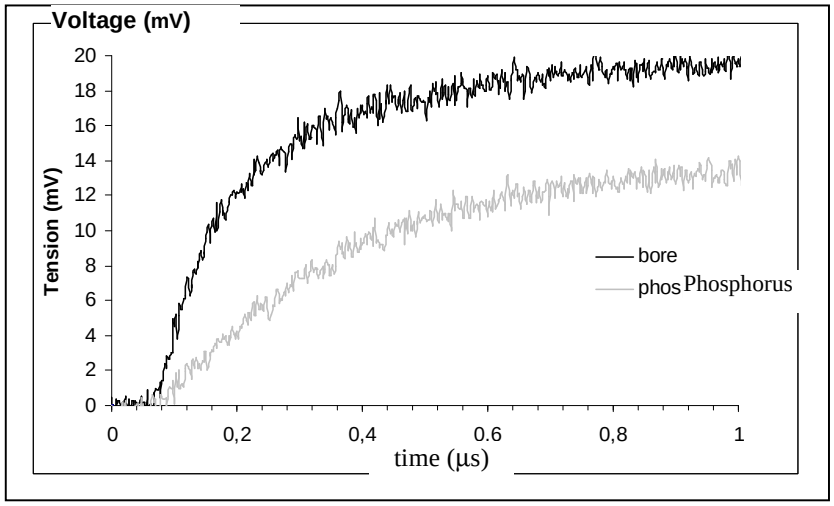

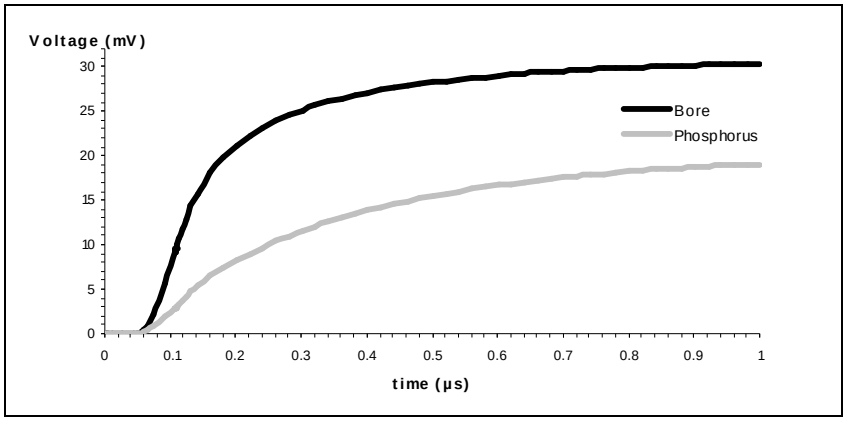

Fig. 10. Above, the experimental responses of two alpha particles arriving at about 1mm near the electrode in bore side ($x \approx 1$, $y=0$) and near the electrode on phosphorus side ($x=0$, $y \approx 1$). Bellow, the corresponding simulated responses with hits of electrode at ($x = 1$, $y = 0$) and at ($x=0$, $y = 1$). We notice a long collection time which is much more than the 10 ns drift time in spite of the input impedance of the CSA equal to zero.

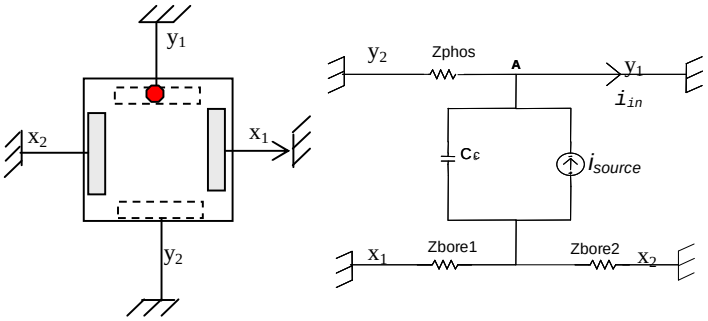

Fig.11. This schematic explains the long collection time phenomena. All the electrodes are connected to the virtual ground. The hit is located onto the electrode y1 and creates the drift current i_{source} between one terminal and the resistive sheet on bore side. The effective time constant of the collected current i_{in} is given by C_c // Z_{bore1} // Z_{bore2}.

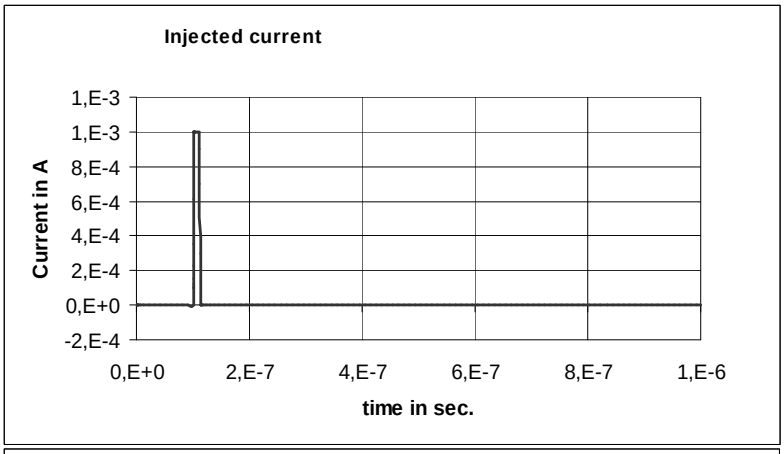

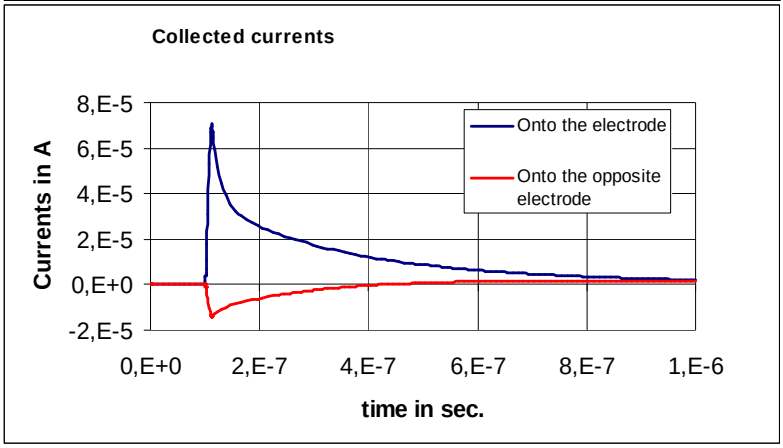

Fig. 12. Above, the injected current i_{source} on a phosphorus electrode (x=0, y=1). Below, the corresponding collected currents i_{phos} through the virtual ground of the preamplifiers which are connected on both phosphorus electrodes. The simulation confirms that the collection is not equal to the 10 ns drift time current. And the current flowing through the opposite electrode is a bipolar pulse with integral zero, (the current turns to positive after 450 ns).

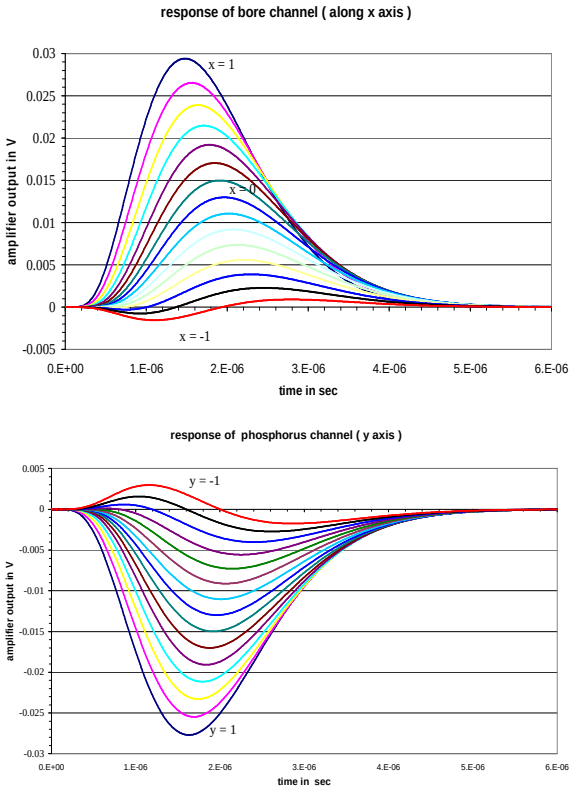

Fig.13: responses of the shaping (spectroscopy) amplifier for hits located along x axe (left) and y axe (right). We notice at the position x = -1, that the wave is negative at the beginning and then become positive instead of staying at zero. (This is the consequence of the "anomalous" negative current.) Therefore the maximum value classically taken to calculate the centroïd is wrong. This explains the distortion near electrodes, where x calculated is less than the position x expected.

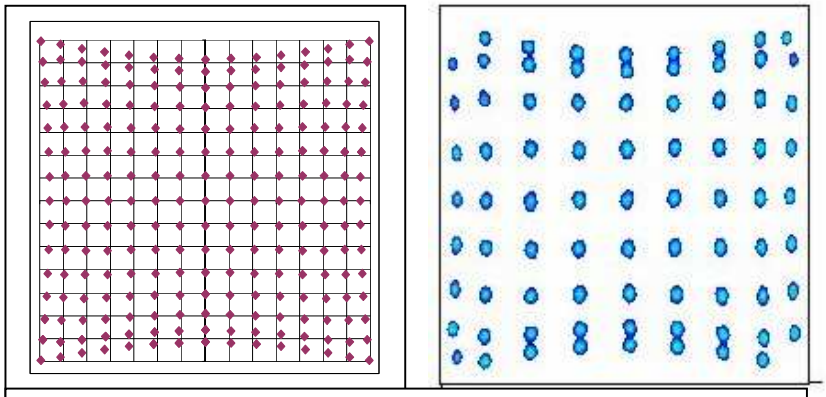

Fig. 14. left: simulated mapping response with shaping amplifier, right: corresponding experimental response at right. In both figures we notice a more important distortion (at edges) in phosphorus side (along y axis). The model reproduces also the week distortion along x axis (bore side). We can also notice that the week barrel non linearities at centre are reproduced by the simulation.

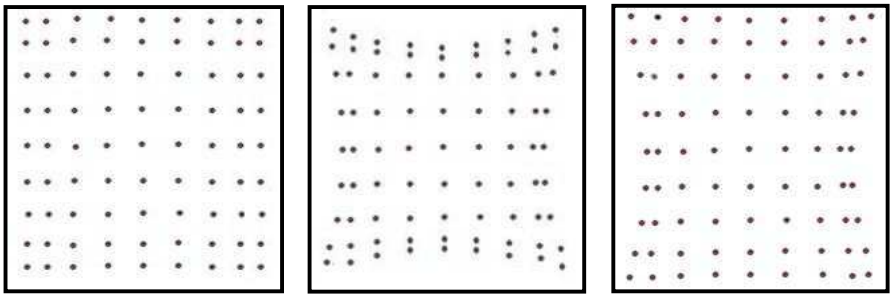

15.a 15.b 15.c

Fig. 15: Experimental PSD mapping for different resistive sheets. 15.a: $R_{ph} = R_{bo} = 4$ kΩ, 15.b: $R_{ph} = R_{bo} = 8$ kΩ, 15.c: $R_{bo} = 4$ kΩ and $R_{ph} = 8$ kΩ. The coupling between resistive sheets is responsible for the deficit ballistic. These experimental figures confirm the prediction model: the distortion in one sheet depend on the resistance of the opposite sheet. The greater is the resistance on one side, greater is the distortion on the other side.